

## Gas-Phase, Bulk Production of Metal Oxide Nanowires and Nanoparticles Using a Microwave Plasma Jet Reactor

Vivekanand Kumar, Jeong H. Kim, Chandrashekhar Pendyala, Boris Chernomordik, and Mahendra K. Sunkara\*

*Department of Chemical Engineering, University of Louisville, Louisville, Kentucky 40292*

*Received: September 3, 2008; Revised Manuscript Received: October 13, 2008*

We report gas-phase production of metal oxide nanowires (NWs) and nanoparticles (NPs) using direct oxidation of micron-size metal particles in a high-throughput, atmospheric pressure microwave plasma jet reactor. We demonstrate the concept with production of SnO<sub>2</sub>, ZnO, TiO<sub>2</sub>, and Al<sub>2</sub>O<sub>3</sub> NWs. The results suggest that the NW production primarily depends upon the starting metal particle size, microwave power, and the gas-phase composition. The resulting NW powders could be separated from the unreacted metal and metal oxide NPs by sonication in 1-methoxy 2-propanol followed by gravity sedimentation. The experiments conducted using higher microwave powers resulted in spherical, unagglomerated, metal oxide NPs. The results obtained using various metal oxides suggest that the mechanism of NW nucleation and growth in the gas phase is similar to that observed in experiments with metal particles supported on substrates. A simplified analysis suggests that the metal powders melt in the plasma primarily with the heat generated from chemical reactions, such as radical recombination and oxidation reactions on the particle surface.

### Introduction

Nanowires (NWs) are beginning to find applications in several fields such as lithium ion batteries,<sup>1</sup> solar cells,<sup>2</sup> optoelectronics,<sup>3</sup> polymer composites,<sup>4</sup> gas sensors,<sup>5,6</sup> nanoelectromechanical devices,<sup>7</sup> etc. Many of these applications require large quantities of NWs, and each may require a particular set of properties. Therefore, bulk synthesis with controlled composition, crystallinity, and morphology is important for continued development and commercialization of NW-based technologies.

Although catalyst assisted vapor–liquid–solid schemes have been typically used to synthesize NWs,<sup>8,9</sup> various other direct reaction schemes have also been demonstrated to synthesize metal oxide NWs, which do not require any foreign catalysts. These include: (i) direct plasma and thermal oxidation of low-melting metal particles supported on substrates using H<sub>2</sub> and O<sub>2</sub> containing gases;<sup>10</sup> (ii) chemical vapor transport of metal oxide vapors onto the substrates in a hot filament chemical vapor deposition (CVD) reactor in atmospheres consisting of low O<sub>2</sub> levels;<sup>11,12</sup> (iii) exposure of metal foils to low-pressure, weakly ionized, fully dissociated, cold O<sub>2</sub> plasmas;<sup>13</sup> (iv) thermal evaporation of metal oxide powders and/or metal oxide powders with carbon onto substrates kept at high temperatures;<sup>14</sup> (v) solution-mediated growth;<sup>15</sup> and (vii) using a directly heated metal foil in air on a hotplate.<sup>16</sup>

Many of the above synthesis methods refer to direct reaction between low melting point metals and O<sub>2</sub>. In some cases, the reaction occurs between micron-size molten metal clusters leading to high density NW growth from the large cluster.<sup>10</sup> In the other cases, metal droplets are formed which initiate self-catalytic tip-led growth of NWs.<sup>17</sup> In all the above cases, the

use of a substrate limits the ability to produce large quantities of NWs using any of the above approaches. The preferred method for high-throughput NW production is gas-phase synthesis, wherein the reacted species are swept away from the reaction zone quickly.

In the case of transition metals with high melting points, rapid oxidation of metal foils in highly dissociated O<sub>2</sub> plasmas can lead to metal oxide NW growth.<sup>13</sup> However, the plasma in this case is not expected to raise the temperature of the metal foils above their melting points. Hence, one-dimensional NW growth in this case was proposed to result from the low mobility of metal atoms. For low-melting metals, both thermal and plasma oxidation of substrate-supported metals occurred at temperatures above the melting point.<sup>10</sup> A recent study showed that Zn powders could be oxidized using high power radio frequency plasma and also DC thermal plasma to produce ZnO NWs.<sup>18,19</sup>

Here, we describe a novel method using a high-throughput plasma jet reactor capable of operating at atmospheric conditions for the direct gas-phase oxidation of metal powders toward bulk NW production at a rate of 5 Kg/day. We studied this process for several metal powders such as Zn, Al, Sn, and Ti with different particle sizes and various plasma parameters.

### Experimental

The experiments were performed in a newly designed reactor that efficiently generates microwave plasma confined inside a quartz tube. The reactor can operate at pressures ranging from a few torr to atmospheric pressures and at powers ranging from 300 W to 3 kW. A schematic and a photograph of the reactor are shown in Figure 1. The reactor also includes a sheath gas delivery chuck to protect the tube from heat generated by high power plasma discharge. This allows for the prolonged operation of the plasma jet. The length of the plasma jet is 12–15 in. as

\* To whom correspondence should be addressed. E-mail: mahendra@louisville.edu. Tel.: 502-852-1558. Fax: 502-852-6355.

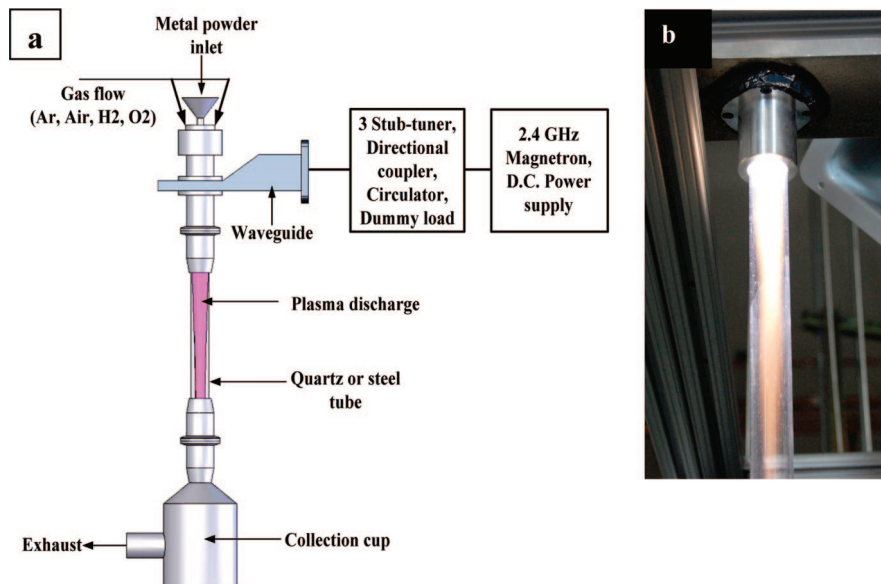


**Figure 1.** (a) Schematic of the microwave plasma jet reactor showing all the essential components. (b) Photograph of the high density plasma jet discharge at 2 kW power produced in a quartz tube of 1.5 in. diameter with a plasma flame length of about 12–15 in.

**TABLE 1: Summary of the Experimental Conditions Used for NW Production**

metal	power, W	flow rates			resulting metal oxide NW characteristics
		air, slpm	H <sub>2</sub> , sccm	O <sub>2</sub> , sccm	
Sn	1200–1500	10–15	100	500	20–100 nm (dia); 10 μm (length)
Zn	1400–1700	10–15	100	500	50–100 nm (dia); 5 μm (length)
Ti	700	8–10	100	500	100–250 nm (dia); 1 μm (length)
Al	800	8–10	100	500	50–150 nm (dia); 3–5 μm in length

shown in Figure 1b. Quartz tubes with diameters of 1.5 and 2 in. are used for the experiments. A metal rod with pointed ends is used to ignite the plasma. Metal powders are poured directly into the plasma cavity zone and then allowed to flow down by gravity with gas flow. Alternatively, there is a provision for feeding the metal source into the plasma jet by pressurized gas, or a mechanical dispenser. The resulting powders are collected at the bottom in either a quartz flask or a filter bag.

Several experiments with different metal powder feeds were conducted in this microwave plasma jet reactor operating at powers ranging from 700 to 2000 W and 2.45 GHz frequency, using 8–15 slpm of air as the sheath gas. Sn and Zn metal powders with a size range of 1–5 μm, Ti powders with a size range of 20–100 μm (65 μm average size), and Al powders with a size range of 3–4.5 μm were used. A gas mixture of 2–4 slpm of Ar and 100–500 sccm of O<sub>2</sub> (the oxidative gas) was used at atmospheric pressures. The resulting metal oxide powders were characterized using a FEI Nova600 FE-SEM, a Renishaw in-via micro-Raman/photoluminescence spectroscope and Bruker D8 Advance model X-ray diffractometer (XRD).

## Results and Discussion

**Different NW Material Systems.** The process conditions with different metal powders and the resulting morphologies are summarized in Table 1. The resulting oxide powders were collected from the quartz cup, filter papers placed in the exhaust, and the quartz tube wall. The powder collected from the filter paper had thinner NWs compared to other powders. The SEM

images in Figures 2a–d show the morphologies of resulting oxide NWs when using Sn and Zn metal powders, respectively. The SnO<sub>2</sub> NWs tend to be straight but highly branched, whereas ZnO NWs have a flowery morphology. Nanostructures of ZnO in the shapes of a tripod, brush, and comb (Figures 2e–g) were also observed. Figures 3a–d show the SEM images of TiO<sub>2</sub> and Al<sub>2</sub>O<sub>3</sub> NWs. TiO<sub>2</sub> NWs are more difficult to synthesize than NPs, and the very short 1D couplet morphology of NWs is obtained, with the current reactor setup. Al<sub>2</sub>O<sub>3</sub> NWs tend to be inverted funnel shaped and protrude out from the bulk metal in a flowery pattern. Straight and isolated Al<sub>2</sub>O<sub>3</sub> NWs have also been observed. The XRD data (shown in the Supporting Information) and the corresponding Raman data (Figure 2h) indicate that the resulting ZnO NWs are composed of the hexagonal wurtzite phase, and SnO<sub>2</sub> NWs are rutile phase.

The experiments using Sn, Zn, and Al metal powders for the respective metal oxide NWs are highly reproducible. However, the experiments using Ti metal powders for NWs are not easily reproducible compared to those for spherical NPs. In the case of Sn and Zn, the product efficiency (the fraction of NWs to NPs) is about 80–90%. The remaining 10–20% is unreacted or partially oxidized metals and agglomerated metal oxide particles.

The above experiments were conducted using a metal powder feed of about 5 g/min which translates to a production capacity of 5 kg of metal oxide NWs per day when operated continuously. The reactor can be operated continuously with a recycle stream for unreacted metal particles and a continuous collection system for metal oxide NWs using filter bags. In any case, the NW production will be limited by two factors: (1) the maximum solid loading in the entraining gas used for recycling; and (2) the maximum amount of solid which can be treated by the plasma flame.

**Post Production Purification.** The resulting powders can contain unreacted metal powder, metal oxide NPs, and metal oxide NWs. These can be purified using a simple gravity sedimentation technique. As an illustration, the as-synthesized ZnO NW powders were dispersed in 1-methoxy 2-propanol, horn sonicated for a few minutes and left for about 4 h under gravity to settle. The top portion of the dispersion contained a high proportion (>95%) of NWs, whereas the bottom precipitate

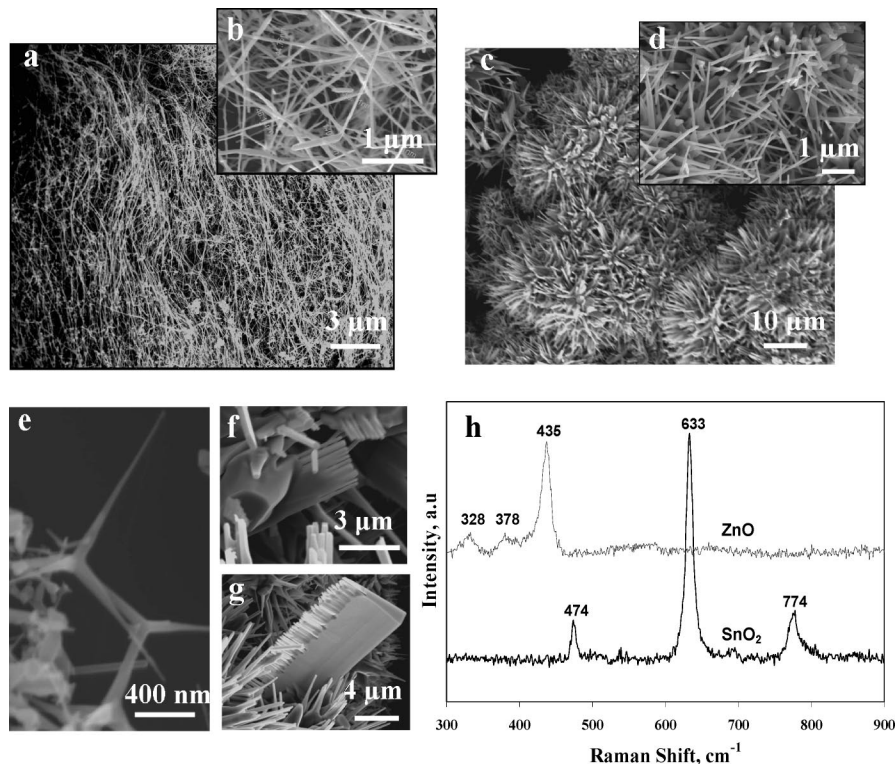


**Figure 2.** Low- and high-resolution SEM images of SnO<sub>2</sub> (a, b) and ZnO (c, d) NWs are shown. Nanostructures of ZnO such as tripod (e), nanobrush (f), and nanocomb (g) were also observed. Raman spectra of as-synthesized SnO<sub>2</sub> and ZnO NWs are shown (h).

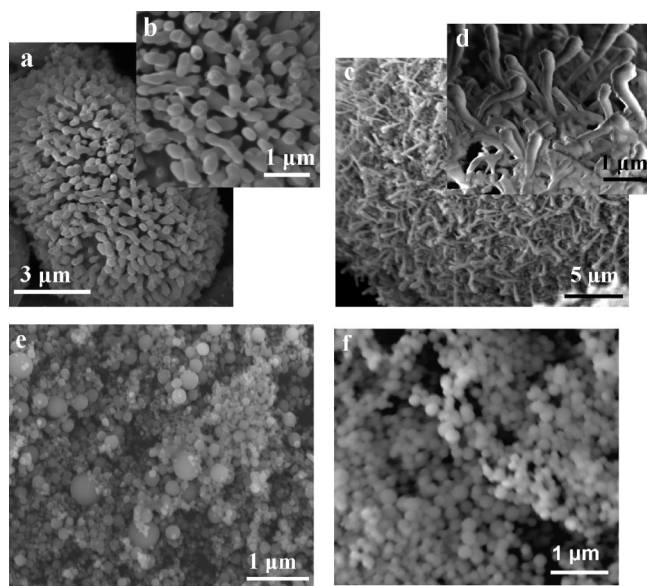


**Figure 3.** Low- and high-resolution SEM images of TiO<sub>2</sub> (a, b) and Al<sub>2</sub>O<sub>3</sub> (c, d) NWs are shown. As-synthesized NPs of TiO<sub>2</sub> (e) and Al<sub>2</sub>O<sub>3</sub> (f) are also shown.

was mostly unreacted metals, partially oxidized metals, and agglomerated metal oxide particles (shown in Supporting Information). The results can be explained based on the agglomeration behavior of spherical particles versus NWs in solutions. In our previous study,<sup>11,20</sup> we studied the dispersion behavior of NPs versus NWs using tungsten oxide and found that the NPs tend to agglomerate into large spherical particles which then settle due to gravity quickly. The NWs if they are not connected with large spherical particles tend to be stable in dispersions.

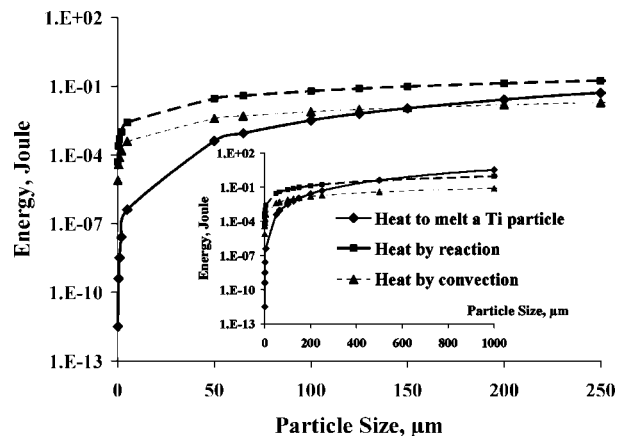


**Figure 4.** Comparison of energy required to melt a Ti metal of 65  $\mu\text{m}$  size and reactive and convective energies imparted to the particle during its fall. Inset shows the comparison at large particle size ranges. The reactive energy is about 10 times higher than the convective energy.

#### Effect of H<sub>2</sub>, Water Vapor, and Metal Powder Diameter.

Experiments were performed using H<sub>2</sub> fed at a rate of 100–500 sccm concurrently along with other gases (approximately 8–12 slpm). In our earlier experiments, using low-pressure microwave plasma and thermal oxidation, the use of H<sub>2</sub>/water vapor helped with both control and low-temperature growth of metal oxide NWs.<sup>10</sup> Experiments conducted using H<sub>2</sub> with Sn metal powders show improved quality, a higher fraction of NWs, and improved size control (about 20 nm diameter) with lengths up to several microns (Figure 2a). Experiments were also conducted by introducing steam as a sheath gas without H<sub>2</sub> as a feed gas. The resulting effect of using water vapor is similar to that using H<sub>2</sub> in the feed gases. The use of H<sub>2</sub> and water in the gas phase produces several active radicals, such as H and OH which can reduce metal oxides. In the presence of such radicals, the lateral growth of metal oxide nuclei is inhibited by maintaining high

surface energy for molten metal.<sup>10</sup> So, the use of H<sub>2</sub> and water vapor helps in reducing the diameter of the resulting NWs. Experiments performed using powders with larger particle sizes (10–100 μm), however, showed a drastic decrease in the fraction of NWs produced. It is thus viable to produce high-quality bulk quantities of NWs using H<sub>2</sub>, water vapor, and small diameter metal powders.

**Production of Metal Oxide NPs versus NWs.** In the case of Ti and Al powders, experiments conducted with 1.3 kW, 10 slpm air, 2 slpm Ar, and 100 and 500 sccm of H<sub>2</sub> and O<sub>2</sub> resulted in the respective metal oxide NPs (Figures 3e,f). In comparison, experiments at lower powers such as 700 and 900 W resulted in NWs. At powers less than 900 W, the resulting Al<sub>2</sub>O<sub>3</sub> NW powders clearly show bulk nucleation and growth of NWs from metal particle cores, as seen in Figure 3. In the case of higher powers, both Ti and Al metal powders were converted into metal oxide vapors, before condensing to form metal oxide NPs. So, spherical NPs were produced at higher plasma power (with high reproducibility) due to the nucleation of a metal oxide particle directly from the condensation of metal oxide vapors, while NWs were produced at lower plasma power due to the nucleation and growth of metal oxide from molten metal particles. Also, the NP production is readily observed in the case of Ti and Al. This is because of high vapor pressures of metal oxide species and the high exothermic heat of surface oxidation and radical recombination reactions. This sometimes also causes irreproducibility in TiO<sub>2</sub> NW experiments. The Al<sub>2</sub>O<sub>3</sub> NPs were more uniform in size compared to TiO<sub>2</sub> NPs because of its smaller metal powder feed size. The XRD spectra of TiO<sub>2</sub> NPs (shown in Supporting Information) indicate that both anatase and rutile phases are present. The anatase fraction (*f<sub>A</sub>*) was calculated to be about 80% using the formula:<sup>21</sup>  $f_A = (1 + 1.265I_R/I_A)^{-1}$ , where *I<sub>R</sub>* and *I<sub>A</sub>* are the strongest peak intensities of rutile and anatase phases in the XRD spectrum of the sample. The Raman spectra (shown in Supporting Information) of the as-synthesized TiO<sub>2</sub> NPs correspond well with that of commercial powders (~95% anatase, from Alfa Aesar) with predominant peaks for the anatase phase and a peak for the rutile phase. The XRD spectra (shown in Supporting Information) of as-synthesized Al<sub>2</sub>O<sub>3</sub> NPs matches with JCPDS database # 016-0394 confirming it to be δ-Al<sub>2</sub>O<sub>3</sub> of tetragonal structure.<sup>22</sup> The δ phase transforms to the α phase upon further heating. This phase does not give Raman bands due to reasons described elsewhere.<sup>23,24</sup>

**Mode of Heating the Metal Particles in Microwave Plasma.** The metal particles cannot absorb microwave radiation directly to get heated. Similarly, the residence time for micron-size metal particles is limited to few seconds. To understand the mode of heating of metal particles, we performed a simple order of magnitude analysis for heat transfer by conduction, convection, radiation, surface chemical reactions, and collisional heating in typical plasma. Our preliminary analysis suggests that convection and reactive heating are the only dominant modes. Collisional heating, which scales with  $v/(\omega^2 + v^2)$ , is ineffective in microwave plasma because the collision to wave frequency ratio  $v/\omega \ll 1$ .<sup>25,26</sup> Here, *v* is the electron-neutral collision frequency and  $\omega$  is the angular frequency of the electromagnetic field. For an electron to collide with a positively charged portion of a metal surface, the time it takes to reach the surface (*1/v*) should be smaller than the time the surface takes to become negatively charged and repulse the electron (*1/ω*, due to changing polarity of microwave-induced electric field).

To melt a 65 μm average size Ti metal particle, 0.9 mJ (milliJoule) of energy ( $mC_p\Delta T + mL$ , *m* is mass of a single spherical particle of Ti, *C<sub>p</sub>* is average specific heat capacity over the temperature range,  $\Delta T$  is the temperature difference between the Ti melting point and ambient temperature, and *L* is the latent heat of fusion) is required. The reactive heating can impart about 40 mJ of energy during a flight time of 0.25 s through the plasma flame. The convective heating, assuming a gas temperature of 1000 K, can provide about 5 mJ to the metal particle. The reactive heating is estimated using the mass flux to the particle, with an average value for heat of reaction of 1000 kJ/mol and 20% contribution by radicals, out of total flux. The most important surface reactions involve O<sub>2</sub> and H<sub>2</sub> radical recombination as well as metal oxidation reactions, which are shown below:

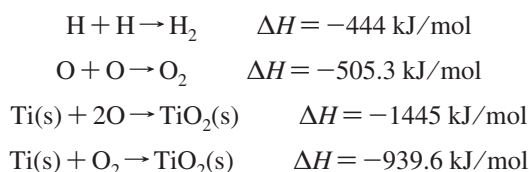


Figure 4 shows the comparison of energy required to melt and the energy supplied via reactive and convective means during the flight as a function of particle size. The data show that the reactive energy is at least an order of magnitude higher than the convective energy. The analysis also shows that there is an upper size limit for the metal particle (in hundreds of microns) beyond which the particles will not melt in plasma using either of the heating modes. Nevertheless, this simple analysis indicates that the reactive heating dominates the overall heating mechanisms for metal particles in microwave plasmas unlike that mentioned in some of the modeling efforts published earlier.<sup>27,28</sup>

To test the hypothesis that the reactive heating is responsible for melting the metal particles, comparative experiments were performed using N<sub>2</sub> plasma at 1.5 kW power and air plasma at 1.2 kW with a gas flow rate of 12 slpm in both cases with the same particle size. The air plasma experiment showed large Ti metal particles getting converted to smaller Ti metal particles along with finer TiO<sub>2</sub> NPs (shown in Supporting Information). The N<sub>2</sub> plasma experiments did not show any significant alteration in the starting metal size. This clearly demonstrates that the metals in plasma are heated to a large extent reactively and not convectively. Convective heating, however, is effective for heating very small size particles. This was confirmed by pouring 100 nm size Zn particles into N<sub>2</sub> plasma at 1.2 kW and 12 slpm flow rate. N<sub>2</sub> plasma treatment of about 10 μm size Al powders, on the other hand, did not show any size modification effect.

**Experimental Observations on Nucleation and Growth of NWs.** Many experiments involving Zn and Al metal powders resulted in flowery morphologies indicating high density of nucleation of metal oxide NWs from large droplets. In many ways, these observations are similar to those observed when performing plasma oxidation of metal particles supported on substrates.<sup>10</sup> The experimental observations with Sn and Ti are slightly different. The flowery type NW growth observed for Ti is not easily reproducible as explained before. In the case of Sn, the resulting NWs are very straight and long (several microns). Experiments with reactive vapor transport of Sn onto substrates<sup>17</sup> also resulted in similar observations of very long, straight, and branched SnO<sub>2</sub> NWs. In the present experiments, such NW growth with direct oxidation of submicron size metal

particles cannot be explained in simple terms and is the subject of our continued studies.

### Conclusions

A generic concept of gas-phase synthesis of metal oxide NWs like ZnO, SnO<sub>2</sub>, TiO<sub>2</sub>, and Al<sub>2</sub>O<sub>3</sub> is demonstrated using an atmospheric microwave plasma jet reactor. The concept can be easily extended to other metal systems. The plasma processing chemistry can also be altered to obtain sulfides, nitrides, carbides, and metal NWs. The introduction of H<sub>2</sub> or steam has been shown to reduce the sizes and increase the yield of NWs in the product. A simple heating model is presented to show that the reactive heating is the dominant mechanism for heating the metal particles in the gas phase.

**Acknowledgment.** Authors gratefully acknowledge support from US Army Space Missile Defense Command (W9113M-04-C-0024), US Department of Energy (DE-FG02-05ER64071 and DE-FG02-05ER64071), and the U.S. Department of Energy/Kentucky Rural Energy Consortium (DE-FG36-05G085013A).

**Supporting Information Available:** XRD spectra of SnO<sub>2</sub> and ZnO NWs; TiO<sub>2</sub> and Al<sub>2</sub>O<sub>3</sub> NPs; Raman spectra of TiO<sub>2</sub> NPs; the results with a purification scheme for NWs from NPs; and experimental results with air and N<sub>2</sub> plasma heating of Ti NPs. This material is available free of charge via the Internet at <http://pubs.acs.org>.

### References and Notes

- (1) Meduri, P.; Pendyala, C.; Kumar, V.; Sumanasekera, G. U.; Sunkara, M. K., under review.
- (2) Gubbala, S.; Chakrapani, V.; Kumar, V.; Sunkara, M. K. *Adv. Funct. Mater.* **2008**, *18*, 2411.
- (3) Huang, Y.; Duan, X.; Lieber, C. M. *Small* **2005**, *1*, 142.
- (4) Vivekchand, S. R. C.; Kam, K. C.; Gundiah, G.; Govindaraj, A.; Cheetham, A. K.; Rao, C. N. R. *J. Mater. Chem.* **2005**, *15*, 4922.

- (5) Deb, B.; Desai, S.; Sumanasekera, G. U.; Sunkara, M. K. *Nanotechnology* **2007**, 285501.
- (6) Cvelbar, U.; Ostrikov, K.; Drenik, A.; Mozetic, M. *Appl. Phys. Lett.* **2008**, *92*, 133505.
- (7) Wang, X.; Song, J.; Liu, J.; Wang, Z. L. *Science* **2007**, *316*, 102.
- (8) Huang, M. H.; Wu, Y.; Feick, H.; Tran, N.; Weber, E.; Yang, P. *Adv. Mater.* **2000**, *13*, 113.
- (9) Dick, K. A.; Deppert, K.; Larsson, M. W.; Martensson, T.; Seifert, W.; Wallenberg, L. R.; Samuelson, L. *Nat. Mater.* **2004**, *3*, 380.
- (10) Sharma, S.; Sunkara, M. K. *J. Am. Chem. Soc.* **2002**, *124*, 12288.
- (11) Thangala, J.; Vaddiraju, S.; Bogale, R.; Thurman, R.; Powers, T.; Deb, B.; Sunkara, M. K. *Small* **2007**, *3*, 890.
- (12) Vaddiraju, S.; Chandrasekaran, H.; Sunkara, M. K. *J. Am. Chem. Soc.* **2003**, *125*, 10792.
- (13) Mozetic, M.; Cvelbar, U.; Sunkara, M. K.; Vaddiraju, S. *Adv. Mater.* **2005**, *17*, 2138.
- (14) Yao, B. D.; Chan, Y. F.; Wang, N. *Appl. Phys. Lett.* **2002**, *81*, 757.
- (15) Jiang, X.; Wang, Y.; Herricks, T.; Xia, Y. *J. Mater. Chem.* **2004**, *14*, 695.
- (16) Yu, T.; Zhu, Y.; Xu, X.; Yeong, K.-S.; Shen, Z.; Chen, P.; Lim, C.-T.; Thong, John, T.-L.; Sow, C.-H. *Small* **2006**, *2*, 80.
- (17) Rao, R.; Chandrasekaran, H.; Gubbala, S.; Sunkara, M.; Daraio, C.; Jin, S.; Rao, A. *J. Electron. Mater.* **2006**, *35*, 941.
- (18) Peng, H.; Fangli, Y.; Liuyang, B.; Jinlin, L.; Yunfa, C. *J. Phys. Chem. C* **2007**, *111*, 194.
- (19) Liao, S.-C.; Lin, H.-F.; Hung, S.-W.; Hu, C.-T. *J. Vac. Sci. Technol., B* **2006**, *24*, 1322.
- (20) Kozan, M.; Thangala, J.; Bogale, R.; Mengu, M. P.; Sunkara, M. K. *J. Nanopart. Res.* **2008**, *10*, 599.
- (21) Spurr, R. A.; Myers, H. *Anal. Chem.* **1957**, *29*, 760.
- (22) Lippens, B. C.; Boer, J. H. d. *Acta Crystallogr.* **1964**, *17*.
- (23) Aminzadeh, A.; Sarikhani-fard, H. *Spectrochim. Acta, Part A* **1999**, *55*, 1421.
- (24) Chen, Y.; Hyldtoft, J.; Jacobsen, C. J. H.; Nielsen, O. F. *Spectrochim. Acta, Part A* **1995**, *51*, 2161.
- (25) Conrads, H.; Schmidt, M. *Plasma Sources Sci. Technol.* **2000**, 441.
- (26) Ganachev, I. P.; Sugai, H. *Plasma Sources Sci. Technol.* **2002**, A178.
- (27) Wan, Y. P.; Prasad, V.; Wang, G.-X.; Sampath, S.; Fincke, J. R. *J. Heat Transfer* **1999**, *121*, 691.
- (28) Fincke, J. R.; Wan, Y. P.; Sampath, S.; Prasad, V.; Herman, H. *Int. J. Heat Mass Transfer* **2002**, *45*, 1007.

JP8078315